Many-body nonequilibrium effects in all-electric electron spin resonance

Jose Reina-Gálvez [*] and Christoph Wolf [†]
Center for Quantum Nanoscience, Institute for Basic Science, Seoul 03760, Korea
and Ewha Womans University, Seoul 03760, Korea

Nicolás Lorente [‡]
Centro de Física de Materiales CFM/MPC (CSIC-UPV/EHU), 20018 Donostia-San Sebastián, Spain
and Donostia International Physics Center, 20018 Donostia-San Sebastián, Spain

(Received 17 March 2023; revised 17 May 2023; accepted 19 May 2023; published 7 June 2023)

Motivated by recent developments in measurements of electron spin resonances of individual atoms and molecules with a scanning tunneling microscope (ESR-STM), we study electron transport through an impurity under periodic driving as a function of the transport parameters in a model junction. The model consists of a single-orbital quantum impurity connected to two electrodes via time-dependent hopping terms. The hopping terms are treated at the lowest order in perturbation theory to recover a Lindblad-like quantum master equation with electron transport. As in the experiment, the ESR-STM signal is given by the variation of the long-time DC current with the driving frequency. The density-matrix coherences play an important role in the evaluation of the ESR-STM signal. Electron correlation is included in our impurity mode. The charging energy U has significant influence on the spin dynamics depending on the sign and magnitude of the applied DC bias. Our model allows direct insight into the origin of the ESR signal from the many-body dynamics of the impurity.

DOI: 10.1103/PhysRevB.107.235404

I. INTRODUCTION

The use of time-dependent techniques in scanning tunneling microscopes (STMs) at gigahertz (GHz) frequencies ushered in the acquisition of electron spin resonances (ESRs) with STMs [1–16]. These developments grant access to new phenomena thanks to the unprecedented high-energy resolution of ESRs combined with the subatomic precision of the STM. Examples include the analysis of elusive atomic configurations on surfaces by measuring the actual magnetic moment of f-electron atoms [2] and the determination of isotopes of single adsorbates [6].

The ESR-STM technique measures the direct current (DC) through a localized spin impurity, such as a single atom or molecule, in the STM junction as the tip-sample bias is periodically modulated. At a certain modulation frequency, the DC current experiences a variation that can be detected. The ESR spectra are values of the junction DC current as a function of driving frequency, typically in the GHz (μeV) range. To drive the localized electron spin, a suitable alternating electric field is fed either directly to the tip [1–11] or to the entire sample via an antenna [1,4]. The mechanism that couples the electric field to a local magnetic moment is not clear, and substantial effort has been devoted to trying to understand under what circumstances an ESR is produced (for a recent review refer to Ref. [17]). Clarifying the origin of ESRs in the STM is not only conceptually but also practically important because full development of the ESR-STM technique requires a high degree of control to acquire meaningful signals.

In the present work, we address the effect of the transport parameters in the ESR signal. Understanding how transport affects the signal yields key information about the way the ESR is produced. In previous publications [18,19], we showed that a time-dependent modulation of the tunneling matrix elements between electrodes and impurity is sufficient to produce a sizable ESR signal. It is well known that electric fields efficiently modulate these transfer matrix elements [20,21], and in turn, this modulation drives the spin [18,19]. Moreover, the suggested adiabatic motion of the impurity in the time-dependent electric field [1,22] would only increase the tunneling modulation. Our model is based on a transport description of the electron current in the presence of driving via the modulation of the tunneling matrix elements. We treat the spin degrees of freedom via a reduced density matrix, which allows us to develop a quantum master equation for the transport process under driving and with quantum spins [19].

The present work includes important differences from Refs. [18,19]. Here, we use a quantum master equation that is correct in the limit of small couplings to the electrodes [23]. However, in Ref. [18], we adopted a simplified two-level system to define a quantum master equation with heuristic rates computed in the cotunneling regime. The present work is consistent in that the quantum master equation implies small couplings and hence a sequential tunneling regime. This approach was already used in Ref. [19], where a simplified $U \to \infty$ impurity model was adopted. Here, we introduce a

[*] galvez.jose@qns.science
[†] wolf.christoph@qns.science
[‡] nicolas.lorente@ehu.eus

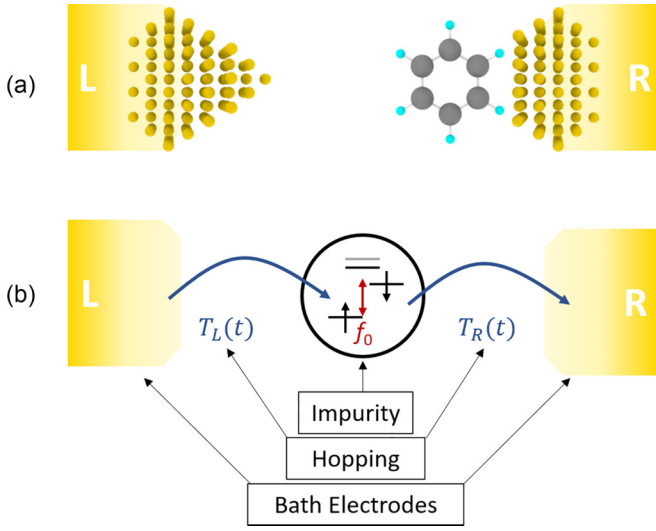

FIG. 1. (a) Scheme of the electron transport geometry for an impurity (here, a molecule) in a junction under an external drive given by the applied bias. In an ESR-STM setup, the left (L) and right (R) electrodes represent the STM tip and substrate. (b) The model used in our Hamiltonian representing the system in (a). A single orbital is connected via time-dependent hopping elements, $T_L(t)$ and $T_R(t)$, to the left and right free-electron electrodes. Under an external magnetic field, the singly occupied spin up ($\uparrow$) and down ($\downarrow$) levels are split by the Zeeman energy with Larmor or resonance frequency f_0. The orbital contains electron-electron correlation by the introduction of a charging energy (or intraorbital Coulomb repulsion) U.

finite charging energy U while keeping the full complexity of the spin degrees of freedom, treated via a spin Hamiltonian. To simplify the discussion of results, we will discuss a spin-1/2 system in the present work.

This paper is organized as follows. In Sec. II, we summarize the model and the theoretical approach. In the present paper, we put special emphasis on clarifying the different equations and on how to treat the extended basis set to include electronic correlations under a finite charging energy U. We present the results of simulations with a set of parameters compatible with experimental ESR-STM setups in Sec. III. The calculations explore the behavior of the continuous-wave (CW) ESR-STM signal (change in DC current as the driving frequency is changed) as a function of the DC bias. The results clearly show the role of the involved states, the importance of having changing populations and coherences, and their influence on the DC current that is ultimately the experimental observable. The results corroborate the importance of coherent charge fluctuations to have a measurable signal in ESR-STM.

II. THEORETICAL APPROACH

Figure 1 shows a representative model of the type of system considered in this work. A central region that can be solved exactly is coupled via some hopping matrix elements to electron reservoirs. These hoppings need to be small compared to the typical energies of the central region in order to obtain a quantum master equation (QME), as will be shown in the following. We solve this QME in the long-time limit using Floquet's theorem, which treats linear differential equations under a periodic drive [24]. Finally, in this section, we derive the equation for the time-dependent electronic current and for its DC component in this long-time limit.

A. The model Hamiltonian

The model for the full quantum system consists of a quantum impurity (a magnetic adsorbate, such as a single atom or molecule) tunnel coupled to two electron reservoirs (see Fig. 1). The full system is described by

$$H(t) = H_{\text{elec}} + H_{\text{I}} + H_{\text{T}}(t), \tag{1}$$

where the first term describes the two electrodes, the second term is the impurity Hamiltonian, and the third term is the tunneling Hamiltonian, which is the only time-dependent one. The electrodes are assumed to be described by one-electron states,

$$H_{\text{elec}} = \sum_{\alpha k\sigma} \varepsilon_{\alpha k} c^{\dagger}_{\alpha k\sigma} c_{\alpha k\sigma}, \tag{2}$$

where α identifies the electrode ($\alpha =$ L,R), $\sigma = \uparrow, \downarrow$ is the electron spin projection along the quantization axis, and k is its momentum. Each electrode is characterized by a chemical potential μ_α such that the total DC bias is $eV_{\text{DC}} = \mu_L - \mu_R$. Following Ref. [19], the quantum impurity consists of a single orbital with intraorbital correlation represented by the charging energy U. The impurity is subjected to an external magnetic field such that its Hamiltonian is given by

$$H_{\text{I}} = \sum_{\sigma} \varepsilon d^{\dagger}_{\sigma} d_{\sigma} + U \hat{n}_{d\uparrow} \hat{n}_{d\downarrow} + g\mu_B \mathbf{B} \cdot \hat{\mathbf{s}}, \tag{3}$$

where ε is the orbital energy of the impurity, U is the corresponding Coulomb repulsion, and $\hat{n}_{d\sigma} = d^{\dagger}_{\sigma} d_{\sigma}$ is the occupation operator of the orbital. Its spin operator $\hat{\mathbf{s}}$ has components $\hat{s}^j = \hbar \sum_{\sigma,\sigma'} d^{\dagger}_{\sigma} \hat{\sigma}^j_{\sigma\sigma'} d_{\sigma'}/2$, where $\hat{\sigma}^j$ ($j = x, y, z$) are the Pauli matrices. The last term of Eq. (3) is the Zeeman contribution to the Hamiltonian.

The coupling between the impurity and the two reservoirs is described by the tunneling Hamiltonian

$$H_T(t) = \sum_{\alpha k\sigma} [T_\alpha(t) c^{\dagger}_{\alpha k\sigma} d_{\sigma} + T^*_\alpha(t) d^{\dagger}_{\sigma} c_{\alpha k\sigma}]. \tag{4}$$

The periodic drive is introduced by a time-dependent hopping $T_\alpha(t)$, parameterized as

$$T_\alpha(t) = T^0_\alpha [1 + A_\alpha \cos(\omega t)], \tag{5}$$

following Refs. [18,19]. This approximation captures the effect of the driving electric field on the electron transfer probability because of the changing tunneling barrier. Figure 2(a) shows a simple scheme for the modulation of the transmission of the wave function across one of the barriers, under varying external electric field. Although not needed, the presence of piezoelectric effects [25] would enhance the tunneling modulation in the time-dependent electric field.

Tunneling modulation is very efficient in driving the spin. In Ref. [18], we showed that the tunneling modulation directly enters the Rabi flip-flop rate in an effective two-level system where electrons hop in and out the impurity. Indeed, the

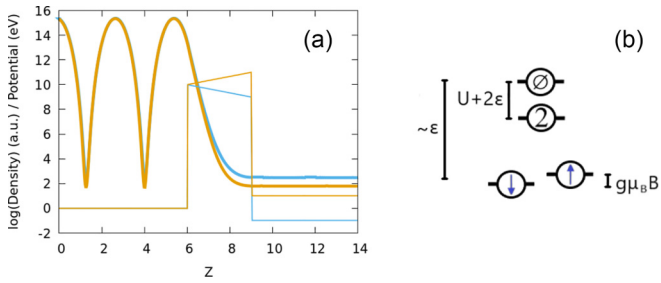

FIG. 2. (a) Barrier modulation, represented here by a one-dimensional barrier along direction z at two different external electric fields. The transmitted wave function (given by the log of the density shown by thick orange and cyan curves corresponding to the two different electric-field values) is much larger for one of the applied biases, illustrating the effect of the *modulation of the hopping* that provides the electric-field coupling to the impurity spin. (b) Energy scheme of the quantum impurity. The four possible states are $|p\rangle = \uparrow, \downarrow, 2, \emptyset$. For representation and discussion purposes, we assume that the eigenstate basis $|l\rangle$ is, in the first approximation, the same as the $|p\rangle$ basis, although all calculations are performed using the numerical eigenstates of the complete impurity Hamiltonian, which can be of considerable complexity. In order to be able to compare the energies of states with different numbers of electrons, we assume that the missing electrons are at the chemical potential of the electrodes at zero bias. The zero-electron state is at zero energy.

tunneling modulation implies an effective change in the state of the impurity due to charge transfer from the electrodes.

To formulate the problem in terms of the reduced density matrix, we consider all possible configurations for zero, one, and two electrons in the impurity. Figure 2(b) shows an energy diagram with the four possible eigenstates of the simplest spin-1/2 system. These configurations are $|p\rangle$, with $p = \uparrow, \downarrow, 2, \emptyset$. The first two account for one-electron states, while the third and fourth label the spin singlets with two and zero electrons, respectively. The impurity Hamiltonian in this basis is given by

$$H_{\rm I} = \sum_p \varepsilon_p |p\rangle\langle p| + \frac{g\mu_B}{2}\{(B_x + iB_y)|\downarrow\rangle\langle\uparrow| + (B_x - iB_y)|\uparrow\rangle\langle\downarrow|\}, \tag{6}$$

where ε_p takes the values $\varepsilon_\sigma = \varepsilon + g\mu_B B_z\sigma$ for $\sigma = \uparrow$ or $\downarrow$, $\varepsilon_2 = 2\varepsilon + U$, and $\varepsilon_\emptyset = 0$. The tunneling Hamiltonian in this $|p\rangle$ basis set is

$$H_T(t) = \sum_{\alpha k\sigma}[T_\alpha(t)c^\dagger_{\alpha k\sigma}|\emptyset\rangle\langle\sigma| + T_\alpha(t)c^\dagger_{\alpha k\sigma}|\bar\sigma\rangle\langle 2| + \text{H.c.}], \tag{7}$$

where $\bar\sigma$ indicates the opposite to the σ spin projection.

Since the impurity Hamiltonian does not depend on time, we can use the eigenbasis of the impurity to describe the reduced density matrix. This eigenstate basis is given by

$$H_{\rm I}|l\rangle = E_l|l\rangle. \tag{8}$$

From now on, Latin characters $(l, j, u, v, \dots)$ refer to eigenstates that are combined electronic and spin configurations of the impurity. Accordingly, we write $H_T(t)$ in terms of the Hubbard operators $|l\rangle\langle j|$ obtained from these impurity many-body eigenstates [26],

$$H_T(t) = \sum_{\alpha k\sigma l j}(T_\alpha(t)c^\dagger_{\alpha k\sigma}\lambda_{lj\sigma}|l\rangle\langle j| + \text{H.c.}),$$

which explicitly contain the matrix element that reflects the change in the many-body configurations of the impurity j of $N+1$ electrons to l of N electrons:

$$\lambda_{lj\sigma} = \langle l|d_\sigma|j\rangle = \langle l|\emptyset\rangle\langle\sigma|j\rangle + \langle l|\bar\sigma\rangle\langle 2|j\rangle. \tag{9}$$

B. The quantum master equation

We derive the QME by treating the coupling between the impurity and the reservoirs to the lowest order in perturbation theory in H_T like in Refs. [19,27–33]. This approximation amounts to the Born-Markov approximation [34,35]). The reduced density matrix in the impurity eigenstate basis set is

$$\rho_{lj}(t) = \text{Tr}[\hat\rho_T(t)|l\rangle\langle j|], \tag{10}$$

with the trace taken over all the degrees of freedom of the total system and $\hat\rho_T(t)$ being the time-dependent density matrix of the total system [19,33].

The QME for $\rho_{lj}(t)$ is directly extracted from [19]

$$\hbar\dot\rho_{lj}(t) - i\Delta_{lj}\rho_{lj}(t) = \sum_{vu}\{[\Gamma_{vl,ju}(t) + \Gamma^*_{uj,lv}(t)]\rho_{vu}(t) - \Gamma_{jv,vu}(t)\rho_{lu}(t) - \Gamma^*_{lv,vu}(t)\rho_{uj}(t)\}, \tag{11}$$

where we have denoted $\Delta_{l,j} = E_l - E_j$. All indices (l, j, v, u) refer only to many-body eigenstates of the impurity Hamiltonian $H_{\rm I}$.

The above QME, Eq. (11), is physically meaningful in the limit of weak coupling between impurity and electrodes. Here, weak means that the induced broadening of the impurity levels is smaller than the typical separation between levels $\Delta_{l,j}$. In this way, we make sure that the dynamics induced by the electrode is a small perturbation of the intrinsic impurity dynamics. In this limit, the different approaches to obtain a linear equation in the reduced density matrix yield the same QME [23].

The rates $\Gamma(t)$ can be written as the sum of two contributions per electrode α:

$$\Gamma_{vl,ju}(t) = \sum_\alpha[\Gamma^-_{vl,ju,\alpha}(t) + \Gamma^+_{vl,ju,\alpha}(t)]. \tag{12}$$

These rates can be expressed as

$$\Gamma^-_{vl,ju,\alpha}(t) = \frac{i}{2\pi}\sum_\sigma \lambda_{vl\sigma}\lambda^*_{uj\sigma}[1 + A_\alpha\cos(\omega t)]\gamma_{\alpha\sigma} \times \int_{-\infty}^{\infty} d\epsilon f_\alpha(\epsilon)\Big(\frac{1}{\epsilon - \Delta_{ju} + i\hbar/\tau_c} + e^{i\omega t}\frac{A_\alpha/2}{\epsilon - \Delta_{ju} + \hbar\omega + i\hbar/\tau_c} + e^{-i\omega t}\frac{A_\alpha/2}{\epsilon - \Delta_{ju} - \hbar\omega + i\hbar/\tau_c}\Big) \tag{13}$$

and

$$\Gamma^{+}_{vl,ju,\alpha}(t) = -\frac{i}{2\pi}\sum_{\sigma}\lambda^{*}_{lv\sigma}\lambda_{ju\sigma}[1+A_\alpha\cos(\omega t)]\gamma_{\alpha\sigma} \times \int_{-\infty}^{\infty} d\epsilon[1-f_\alpha(\epsilon)]\Bigg(\frac{1}{\epsilon+\Delta_{ju}-i\hbar/\tau_c} + e^{i\omega t}\frac{A_\alpha/2}{\epsilon+\Delta_{ju}+\hbar\omega-i\hbar/\tau_c} + e^{-i\omega t}\frac{A_\alpha/2}{\epsilon+\Delta_{ju}-\hbar\omega-i\hbar/\tau_c}\Bigg). \quad (14)$$

The Fermi occupation function is given by $f_\alpha(\epsilon) = 1/(e^{\beta_\alpha(\epsilon-\mu_\alpha)}+1)$, where β_α is the inverse temperature times the Boltzmann constant for electrode α. Additionally, $\gamma_{\alpha\sigma}$ is the level broadening due to the hopping T^0_α to electrode α for spin σ:

$$\gamma_{\alpha\sigma} = 2\pi D_{\alpha\sigma}\left|T^0_\alpha\right|^2, \quad (15)$$

which depends on the spin-dependent density of states, given by

$$D_{\alpha\sigma} = D_\alpha(1/2+\sigma P_\alpha). \quad (16)$$

Here, $\sigma = \pm 1/2$, P_α is a real number between -1 and 1 giving the spin polarization of the electrode, and D_α is the density of states of the electrode at the Fermi energy.

The above rate expressions neglect the time dependence of the electrodes [19]. This approximation is valid when the AC amplitude is much smaller than the DC component of the bias; otherwise, Eq. (13) should include further Bessel functions to take into account the time dependence of the electrode's Green's function [20,21].

The physical interpretation of the rates is straightforward. The rates are proportional to $\gamma_{\alpha\sigma}$, Eq. (15), which is the usual broadening induced by the hopping-matrix elements and the density of states of the electrodes. Whether the process involves electrons or holes is contained in the appearance of the Fermi occupation factors. The expressions given in Eqs. (13) and (14) contain the λ matrix elements that take in the right weights of each impurity state. Finally, the factors including the magnitude of the hopping modulation A_α take into account whether the electron-transfer process involves the absorption or emission of a photon from the microwave field.

Finally, a finite $1/\tau_c$ improves the convergence of the Green's function. Its inclusion leads to a small renormalization (or Lamb shift) of the spectrum. The value of this number is crucial as it affects the imaginary part of the Green's function and has a significant impact on the overall dynamics. As with any numerical implementation, it is essential to be careful with the chosen values, particularly for a quantity that should be infinitesimal. To ensure accuracy, we verify all our calculations against variations in $1/\tau_c$.

C. The long-time limit

The rate is periodic in time at a fixed drive of frequency $\omega/2\pi$ and can be expanded in terms of Fourier components, allowing us to express all equations in Floquet components. We introduce the Floquet index n as the Fourier index of the rate [24]:

$$\Gamma_{vl,ju,\alpha}(t) = \sum_n e^{-in\omega t}\,\Gamma_{vl,ju,\alpha;n}(\omega). \quad (17)$$

From Eqs. (11) and (17), we can write the Floquet master equation,

$$\Delta_{lj}\rho_{lj;n} + n\hbar\omega\rho_{lj;n} = i\sum_{vu;n'}\{[\Gamma_{vl,ju;n'}(\omega)+\Gamma^{*}_{uj,lv;-n'}(\omega)]\rho_{vu;n-n'} - \Gamma^{*}_{lv,vu;-n'}(\omega)\rho_{uj;n-n'} - \Gamma_{jv,vu;n'}(\omega)\rho_{lu;n-n'}\}. \quad (18)$$

D. Expressions for the electronic current

The current flowing out of electrode α is defined as $I_\alpha = -e\frac{d\langle N_\alpha\rangle}{dt}$. This translates into the usual Meir-Wingreen formula [36], where now the matrix elements of all quantities appear in terms of many-body eigenstates, l, j, and u (see Ref. [19]):

$$I_\alpha(t) = \frac{2e}{\hbar}\sum_{lju}\mathrm{Re}\{\rho_{lu}(t)[\Gamma^{-}_{lj,ju,\alpha}(t)-\Gamma^{+}_{lj,ju,\alpha}(t)]\}. \quad (19)$$

Using $I_L = -I_R$, we symmetrize the current by setting $I = (I_L+I_L)/2 = (I_L-I_R)/2$, and the above expression can be rewritten as

$$I(t) = -\frac{2e}{\hbar}\sum_{lju}\mathrm{Re}\{\rho_{lu}(t)[\Gamma^{-}_{lj,ju,R}(t)+\Gamma^{+}_{lj,ju,L}(t) - \Gamma^{-}_{lj,ju,L}(t)-\Gamma^{+}_{lj,ju,R}(t)]\}. \quad (20)$$

This expression differs from previous approaches because it now contains the contribution of the coherences of the density matrix, not only the populations [37–39]. We will show that under certain conditions the coherences are crucial for the correct calculation of the ESR signal.

Since CW ESR-STM experiments measure the DC current in the long-time limit, we express it in Floquet components as

$$I(\omega) = -\frac{2e}{\hbar}\sum_{lju;n'}\mathrm{Re}\{\rho_{lu;-n'}(\omega)[\Gamma^{-}_{lj,ju,R;n'}+\Gamma^{+}_{lj,ju,L;n'} - \Gamma^{-}_{lj,ju,L;n'}-\Gamma^{+}_{lj,ju,R;n'}]\}. \quad (21)$$

Finally, let us emphasize that a full description based on a QME is possible when keeping to the lowest order in the hopping terms. This order is sufficient when the impurity level lies within the two Fermi levels. However, outside this bias window, higher-order terms may become comparable to or larger than the lower-order term. These higher-order terms contain sums over intermediate states, opening the possibility of cotunneling processes and of Kondo scattering (see, for example, Refs. [18,40,41]). In the present approach these processes are absent.

III. RESULTS

Our model consists of an $S = 1/2$ impurity that is weakly connected to two electrodes under a finite DC bias and a CW drive. Our aim is to explore the behavior of the ESR signal as the DC voltage is varied for a set of parameters intended to mimic conditions found in ESR-STM experiments.

A. Model parameters

The model parameters are chosen under the proviso of obtaining a strong ESR signal of an $S = 1/2$ system weakly connected to two electrodes under electrical driving. To achieve this, we need the following: (1) an imbalance in the transport-electron spin in order to make the main rates different from zero, which is achieved by having different spin polarizations of the electrodes; (2) a predominant long-time average population of one electron in the impurity so that the system does not behave like a $S = 1/2$ system; (3) an electronic level ε within the DC-bias range; (4) to flip the transport spin using a magnetic field transverse to the electron spin polarization; (5) a modulation of the tunneling hopping with the spin-polarized electrode by the oscillating electric field; and (6) a low temperature (we take 1 K for both electrodes).

In our calculations, we achieve the above conditions with the following parameters: (1) The left electrode has a polarization of $P_L = 0.45$ in Eq. (16). Increasing the polarization up to 100% will increase the ESR signal amplitude. (2) To stabilize the charge state, we apply different couplings with $\gamma_R = 20 \times \gamma_L = 5$ μeV. This coupling asymmetry is often found in experiments, where the impurity couples more strongly to the substrate than the STM tip. The DC bias drop is $eV_{\rm DC} = \mu_L - \mu_R$. We use the model of a double-barrier tunnel junction [42] and assume an asymmetric DC bias drop where $\mu_L = (1-\eta)eV_{\rm DC}$ and $\mu_R = -\eta eV_{\rm DC}$ with the factor $\eta = \gamma_L/(\gamma_L+\gamma_R) = 1/21$. This means that the bias drop takes places mostly on the left electrode. (3) The energy of our model is set to $\varepsilon = -10$ meV. In addition, the electronic states are assumed to have an intrinsic width of $\hbar/\tau_c = 10$ μeV. In order to explore the interplay of the many-body states in ESR processes, we take a fixed charging energy close to the electronic level energy of $U = 3|\varepsilon|/2 = 15$ meV. (4) In order to flip the spin, defined along the z axis of the spin polarization P_L, we apply a B-field component along the x axis perpendicular to the z-axis component. The magnetic field is taken as $\mathbf{B} = (0.6, 0, 0.1)$ T, which gives a Larmor frequency of approximately 17 GHz. The largest ESR signal takes place for a magnetic field completely aligned with the x axis, in good agreement with experiments [16]. (5) The modulation of the tunneling matrix element is $A_L = 50\%$, Eq. (5), and applied only to the left electrode, which is the polarized one. Since the right electrode is not spin polarized, A_R does not contribute to the resonance, only to the background current.

B. Nonzero rates: The opening of transport channels with applied bias

A transport channel opens when the corresponding rates, Eq. (12), are different from zero. Inspection of Eq. (13) shows that this occurs when two conditions are met: The first one is energy conservation, largely controlled by the Fermi factors. The energy conservation implies that the change in state has to be compensated by the applied bias. Under our present conditions, the bias drop takes place largely at the left electrode; then $\Delta_{v,l} = E_v - E_l$ has to be larger than $\mu_L = eV_L = (1-\eta)eV_{\rm DC}$. This is due to the appearance of the term $f(\Delta_{v,l})$ in Eq. (13) when $1/\tau_c \to 0^+$. The second condition is that the sequential transport process leads to a change in the charge state of the impurity such that $\lambda_{vl\sigma} \neq 0$ when v and l differ in one electron of spin σ. Then, the difference in energy $\Delta_{v,l}$ in the rates (12) always addresses states differing by one electron.

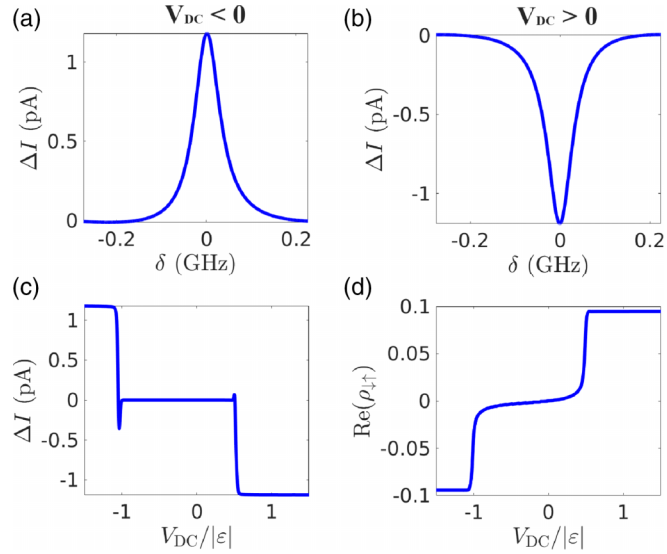

FIG. 3. (a) and (b) ESR signal $\Delta I(f) = I(f) - I_{\rm BG}$ as a function of relative frequency $\delta = f - f_0$ for two different signs of the DC bias. In (a) the DC bias is negative, and in (b) the DC bias is positive, which inverts the ESR amplitude. f_0 is the natural resonance frequency of the Hamiltonian (Larmor frequency) plus the renormalization imposed by the Lamb shift. (c) ESR signal and (d) real part of the coherence $\rho_{\uparrow\downarrow}$ between spin up and down as a function of DC bias when on resonance ($\delta = 0$). The transport channels are closed for $V_{\rm DC} \lesssim U + \varepsilon$ (neglecting the Zeeman energy) and $V_{\rm DC} \geqslant \varepsilon$. In this work we took $U = 3|\varepsilon|/2$, so the ESR signal is zero between $V_{\rm DC}/|\varepsilon| \lesssim 0.5$ and $V_{\rm DC}/|\varepsilon| \geqslant -1$. The behavior of the ESR signal reflects the behavior of the coherences except for a sign.

C. DC-bias dependence of the ESR signal

The DC bias will determine when the transport channels of the system open. But the occurrence of ESR further depends on the possibility of a spin-flip process. For this, the transport channel must be compatible with spin-flip processes.

First, we study the dependence of the magnitude and sign of the ESR signal ΔI as a function of the magnitude and sign of the applied DC bias. Figures 3(a) and 3(b) show two representative spectra taken at opposite signs of the DC bias. The difference between the two spectra is more than a change in sign. To better understand this behavior, Fig. 3(c) shows the ESR peak intensity as a function of $V_{\rm DC}$. Take, for example, a positive bias where we obtain a large negative value of the ESR signal. This correlates with a large contribution of the coherence term $\rho_{\uparrow\downarrow}$ between spin up and down [Fig. 3(d)]. We emphasize that this occurs in the long-time limit under substantial decoherence of the system as long as the drive sustains the coherences. The connection between the ESR signal and coherences of the density matrix can be understood by studying the behavior of the electronic current, Eq. (19).

When the applied bias is positive ($\mu_L - \mu_R > 0$), spin-polarized electrons flow from the left electrode into the impurity. A negative ion is formed if $\mu_L > \Delta_{2,\downarrow} = E_2 - E_\downarrow \approx$

$U + \epsilon$ (we have neglected the Zeeman energy), which corresponds to a transition from a singly occupied level (with spin down, $u = \downarrow$) to a doubly charged level ($v = 2$). At the same time, we need $\mu_R < \Delta_{2,\downarrow}$, which is the case at positive bias. Similarly, the formation of the positively charged ion is energetically possible. However, there is an important asymmetry due to the very different couplings between impurity and electrodes ($\gamma_L \ll \gamma_R$) as well as in the bias drop. As a consequence the formation of the negative ion is favored over the positive one for the present case. Then, we can simplify the expression for the electron current, Eq. (19), by neglecting the involvement of the positive ion and considering only the negative ion as the intermediate step in the electron transfer between electrodes through the impurity:

$$I(\omega) = \frac{2e}{\hbar}\mathrm{Re}\{\rho_\downarrow(\omega)\Gamma^-_{\downarrow 2,2\downarrow,L;0} + \rho_\uparrow(\omega)\Gamma^-_{\uparrow 2,2\uparrow,L;0} + \rho_{\downarrow,\uparrow}(\omega)\Gamma^-_{\downarrow 2,2\uparrow,L;-1} + \rho_{\uparrow,\downarrow}(\omega)\Gamma^-_{\uparrow 2,2\downarrow,L;1}\}, \quad (22)$$

where, for instance, $\Gamma^-_{\downarrow 2,2\downarrow,L;0}$ is the electron rate for a process that involves a non-spin-flip transition (spin-up state) through the doubly occupied one by exchanging an electron with the left electrode, Floquet index $n = 0$. At the same time, $\rho_\downarrow = \rho_{\downarrow\downarrow,0}$, while $\rho_{\downarrow\uparrow} = \rho_{\downarrow\uparrow,1}$ and $\rho_{\uparrow\downarrow} = \rho_{\uparrow\downarrow,-1}$, where $-1, 0, 1$ are Floquet indices.

At a large enough bias, all channels are open, giving a background current I_{BG}:

$$I_{\mathrm{BG}} = \frac{2e}{\hbar}\mathrm{Re}\{\rho_\downarrow(\omega)\Gamma^-_{\downarrow 2,2\downarrow,L;0} + \rho_\uparrow(\omega)\Gamma^-_{\uparrow 2,2\uparrow,L;0}\},$$

which recovers the usual expression for the current for very asymmetrical couplings [36]. The background current shows a small frequency dependence as it is largely given by the rates with Floquet index $n = 0$. Indeed, there is no coherence in the density matrix when the driving frequency is different from the Larmor frequency (off resonance) and $I(\omega) = I_{\mathrm{BG}}$.

Only on resonance is the coherence $\rho_{\downarrow,\uparrow}(\omega)$ different from zero. Then, there is a clear frequency-dependent contribution to the current at the Larmor frequency that originates in the coherences of the density matrix. Accordingly, the coherence contribution to the DC current depends on the Floquet indices $n = \pm 1$.

Increasing the value of the charging energy U moves the doubly occupied state energy ($E_2 = 2\epsilon + U$). For $U \to +\infty$, it becomes impossible to open the channel connecting the single-electron states with the doubly occupied one. As a consequence, the ESR signal completely disappears for positive bias.

At negative bias, $\mu_L < \Delta_{\downarrow,\emptyset} = -10$ meV marks the threshold for having a current, where $v = \emptyset$ corresponds to the positively charged impurity. As in the discussion above, we have neglected the Zeeman energy. The ESR signal also follows the behavior of $-\rho_{\uparrow\downarrow}$ as above (Fig. 3).

The intermediate state mediating the transport process at negative bias is the one corresponding to the positive ion, $v = \emptyset$. Then Eq. (19) can be simplified by taking the positive ion contribution:

$$I(\omega) = -\frac{2e}{\hbar}\mathrm{Re}\{\rho_\downarrow(\omega)\Gamma^+_{\downarrow\emptyset,\emptyset\downarrow,L;0} + \rho_\uparrow(\omega)\Gamma^+_{\uparrow\emptyset,\emptyset\uparrow,L;0} + \rho_{\downarrow,\uparrow}(\omega)\Gamma^+_{\downarrow\emptyset,\emptyset\uparrow,L;-1} + \rho_{\uparrow,\downarrow}(\omega)\Gamma^+_{\uparrow\emptyset,\emptyset\downarrow,L;1}\}, \quad (23)$$

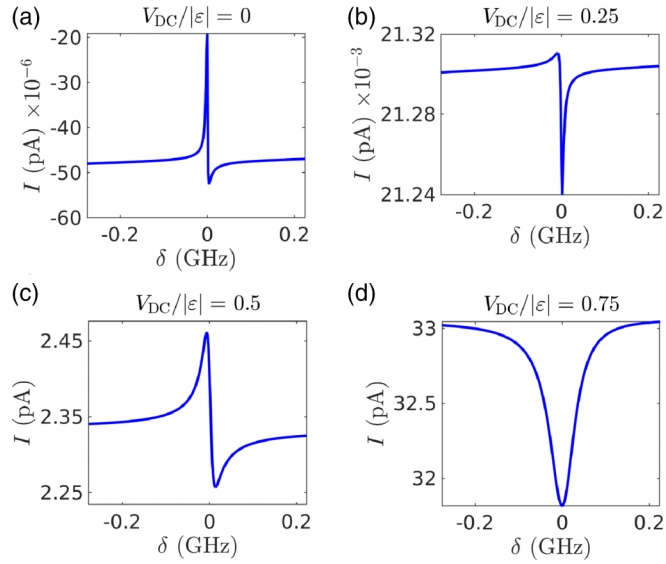

FIG. 4. DC current as a function of the driving frequency $\delta = f - f_0$ for the four different positive voltages: (a) $V_{\mathrm{DC}} = 0$, (b) $V_{\mathrm{DC}} = 2.5$ mV, (c) $V_{\mathrm{DC}} = 5$ mV, and (d) $V_{\mathrm{DC}} = 7.5$ mV. The background current was not removed. The current changes in a small interval about the resonance frequency. For DC bias below the threshold (at 5 mV here) the DC current drops dramatically as the channel closes and the line shape as a function of frequency becomes increasingly asymmetric. Moreover, the width of the resonance also increases with the DC bias, leading to smaller T_2 times as the decoherence is enhanced. The more asymmetric Fano profiles are found near the transport-channel thresholds.

where, again, the ESR signal originates in the coherences of the density matrix. Contrary to the positive-bias case, the limit $U \to \infty$ does not alter the results since the doubly occupied level is not involved.

There is a strong connection between the charging energy and the bias dependence. Only at the symmetric point, when $\varepsilon = -U/2$, is perfect electron-hole symmetry achieved, and the ESR signal becomes symmetric with respect to the bias sign. At $U \to \infty$ the electron-hole asymmetry becomes the largest, with no ESR signal for positive bias and a large signal for negative bias at the bias threshold marked by the impurity level. This highlights the important role of the charging energy in determining the bias dependence and ESR-STM measurements.

D. ESR-STM linewidths

Figure 4 shows four characteristic CW ESR-STM signals as a function of the frequency of the drive, $f = \omega/2\pi$, for positive DC bias. At threshold, $V_{\mathrm{DC}} \approx U + \varepsilon \approx 5$ mV, a strongly asymmetric Fano profile is obtained. This behavior can be traced back to the interference between the on-resonance scattering with the background. As the bias is further reduced, the transmission channel is increasingly closed, leading to a smaller background current and a smaller signal. In this regime, the ESR signal also depends on the change in the populations, in stark contrast to the open-channel case, where the ESR signal is basically determined by the coherences.

Furthermore, the closed-channel region is particularly intriguing due to its potential for enhancing coherence, particularly when higher-order transport processes such as cotunneling are not dominant. Experimental evidence, as reported in Ref. [4], has demonstrated that the flow of electronic current is a significant source of decoherence. However, when the current is reduced, such as in the closed-channel region, there is improved coherence in the spin evolution.

The current approach to studying this regime is valid as long as cotunneling and other higher-order transport processes are not dominant. This brings attention to two important points. First, we emphasize the presence of a closed-channel region, where even minor changes in population can significantly affect the current. Second, this region is characterized by long decoherence times, making it highly desirable for experimental purposes.

IV. SUMMARY AND CONCLUSIONS

This work explored the ESR signal in the DC current through a quantum impurity connected to two electron reservoirs under bias. The model is intended to reproduce the conditions of ESR-STM, where the applied bias contains a DC component and an AC component usually in the GHz frequency range. We extended previous work [19] to include finite intra-atomic correlation, and we showed its impact on the DC-bias dependence of the ESR signal. Our theory is based on a Linblad-like QME that was obtained by keeping the modulation of the tunneling matrix element to lowest order. This limits the transport regime to the sequential or on-resonance one. This situation seems to be similar to transition-metal impurities, molecules, and alkali metal dimers that have s electrons close to the Fermi energy of the substrate [43–46]. We treated only spin-1/2 systems in the present study, but the extension to larger spin systems can be achieved with relative ease.

Our choice for ε and charging energy U values breaks the electron-hole symmetry of the system. This has wide-ranging implications for the transport when taking into account the opening and closing of different transport channels as the applied DC bias varies. As a consequence, spin-1/2 systems such as the ones in Refs. [43–46] should exhibit a bias-sign dependence of the ESR signal in the experiment.

Our work highlights the importance of properly including the complete reduced density matrix in the calculation of the ESR signal. In the open-channel case, we found that the ESR signal is proportional to the coherences or off-diagonal elements of the density matrix. However, in the closed-channel region, the diagonal elements or populations play a significant role. Therefore, the ESR-induced change in the DC current can be indicative of coherences or population changes of the system depending on the transport regime.

The present theory is based on a charge-fluctuation description in which the impurity charge changes during the electron transport process and the fluctuations induce the spin-flip processes that, in turn, lead to the ESR signal as long as driving and polarization are maintained. Our results emphasize the need to correctly treat the coherent charge fluctuation and include the coherence in the description of the full transport processes, not only for the evaluation of the impurity's population but also in the equation for the electron current.

ACKNOWLEDGMENTS

We are pleased to thank our collaborators for important discussions. A nonexhaustive list of the many contributors to our discussions includes L. Arrachea, D.-J. Choi, F. Delgado, F. Donati, J.-P. Gauyacq, A. J. Heinrich, and S.-H. Phark. This work was supported by the Institute for Basic Science (Grant No. IBS-R027-D1). Further financial support from the Spanish State Research Agency Projects No. RTI2018-097895-B-C44 and No. PID2021-127917NB-I00 funded by Grant No. MCIN/AEI/10.13039/501100011033 is gratefully acknowledged. We also thank the Basque Government for project No. IT-1527-22. Funding was provided by the European Union. Views and opinions expressed are, however, those of the author(s) only and do not necessarily reflect those of the European Union. Neither the European Union nor the granting authority can be held responsible for them.

[1] S. Baumann, W. Paul, T. Choi, C. P. Lutz, A. Ardavan, and A. J. Heinrich, Science **350**, 417 (2015).
[2] F. D. Natterer, K. Yang, W. Paul, P. Willke, T. Choi, T. Greber, A. J. Heinrich, and C. P. Lutz, Nature (London) **543**, 226 (2017).
[3] T. Choi, W. Paul, S. Rolf-Pissarczyk, A. J. Macdonald, F. D. Natterer, K. Yang, P. Willke, C. P. Lutz, and A. J. Heinrich, Nat. Nanotechnol. **12**, 420 (2017).
[4] P. Willke, W. Paul, F. D. Natterer, K. Yang, Y. Bae, T. Choi, J. Fernández-Rossier, A. J. Heinrich, and C. P. Lutz, Sci. Adv. **4**, eaaq1543 (2018).
[5] K. Yang, Y. Bae, W. Paul, F. D. Natterer, P. Willke, J. L. Lado, A. Ferrón, T. Choi, J. Fernández-Rossier, A. J. Heinrich, and C. P. Lutz, Phys. Rev. Lett. **119**, 227206 (2017).
[6] P. Willke, Y. Bae, K. Yang, J. L. Lado, A. Ferrón, T. Choi, A. Ardavan, J. Fernández-Rossier, A. J. Heinrich, and C. P. Lutz, Science **362**, 336 (2018).
[7] Y. Bae, K. Yang, P. Willke, T. Choi, A. J. Heinrich, and C. P. Lutz, Sci. Adv. **4**, eaau4159 (2018).
[8] P. Willke, A. Singha, X. Zhang, T. Esat, C. P. Lutz, A. J. Heinrich, and T. Choi, Nano Lett. **19**, 8201 (2019).
[9] P. Willke, K. Yang, Y. Bae, A. Heinrich, and C. Lutz, Nat. Phys. **15**, 1005 (2019).
[10] K. Yang, W. Paul, F. D. Natterer, J. L. Lado, Y. Bae, P. Willke, T. Choi, A. Ferrón, J. Fernández-Rossier, A. J. Heinrich, and C. P. Lutz, Phys. Rev. Lett. **122**, 227203 (2019).
[11] K. Yang, W. Paul, S.-H. Phark, P. Willke, Y. Bae, T. Choi, T. Esat, A. Ardavan, A. J. Heinrich, and C. P. Lutz, Science **366**, 509 (2019).
[12] T. S. Seifert, S. Kovarik, C. Nistor, L. Persichetti, S. Stepanow, and P. Gambardella, Phys. Rev. Res. **2**, 013032 (2020).
[13] T. S. Seifert, S. Kovarik, D. M. Juraschek, N. A. Spaldin, P. Gambardella, and S. Stepanow, Sci. Adv. **6**, eabc5511 (2020).

[14] W. M. J. van Weerdenburg, M. Steinbrecher, N. P. E. van Mullekom, J. W. Gerritsen, H. von Allwörden, F. D. Natterer, and A. A. Khajetoorians, Rev. Sci. Instrum. **92**, 033906 (2021).
[15] M. Steinbrecher, W. M. J. van Weerdenburg, E. F. Walraven, N. P. E. van Mullekom, J. W. Gerritsen, F. D. Natterer, D. I. Badrtdinov, A. N. Rudenko, V. V. Mazurenko, M. I. Katsnelson, A. van der Avoird, G. C. Groenenboom, and A. A. Khajetoorians, Phys. Rev. B **103**, 155405 (2021).
[16] J. Kim, W. J. Jang, T. H. Bui, D. J. Choi, C. Wolf, F. Delgado, Y. Chen, D. Krylov, S. Lee, S. Yoon, C. P. Lutz, A. J. Heinrich, and Y. Bae, Phys. Rev. B **104**, 174408 (2021).
[17] F. Delgado and N. Lorente, Prog. Surf. Sci. **96**, 100625 (2021).
[18] J. Reina Gálvez, C. Wolf, F. Delgado, and N. Lorente, Phys. Rev. B **100**, 035411 (2019).
[19] J. Reina-Gálvez, N. Lorente, F. Delgado, and L. Arrachea, Phys. Rev. B **104**, 245435 (2021).
[20] A.-P. Jauho, N. S. Wingreen, and Y. Meir, Phys. Rev. B **50**, 5528 (1994).
[21] L. Arrachea and M. Moskalets, Phys. Rev. B **74**, 245322 (2006).
[22] J. L. Lado, A. Ferrón, and J. Fernández-Rossier, Phys. Rev. B **96**, 205420 (2017).
[23] C. Timm, Phys. Rev. B **77**, 195416 (2008).
[24] M. Grifoni and P. Hänggi, Phys. Rep. **304**, 229 (1998).
[25] S.-H. Phark, Y. Chen, C. Wolf, H. T. Bui, Y. Wang, M. Haze, J. Kim, C. P. Lutz, A. J. Heinrich, and Y. Bae, arXiv:2108.09880.
[26] A. C. Hewson, *The Kondo Problem to Heavy Fermions* (Cambridge University Press, Cambridge, 1997).
[27] H. Schoeller and G. Schön, Phys. Rev. B **50**, 18436 (1994).
[28] J. König, H. Schoeller, and G. Schön, Phys. Rev. Lett. **76**, 1715 (1996).
[29] J. König, J. Schmid, H. Schoeller, and G. Schön, Phys. Rev. B **54**, 16820 (1996).
[30] J. Splettstoesser, M. Governale, J. König, and R. Fazio, Phys. Rev. B **74**, 085305 (2006).
[31] M. Esposito and M. Galperin, Phys. Rev. B **79**, 205303 (2009).
[32] F. Cavaliere, M. Governale, and J. König, Phys. Rev. Lett. **103**, 136801 (2009).
[33] B. Bhandari, R. Fazio, F. Taddei, and L. Arrachea, Phys. Rev. B **104**, 035425 (2021).
[34] J. Rammer, *Quantum Field Theory of Non-equilibrium States* (Cambridge University Press, Cambridge, 2007).
[35] G. Dorn, E. Arrigoni, and W. von der Linden, J. Phys. A **54**, 075301 (2021).
[36] Y. Meir and N. S. Wingreen, Phys. Rev. Lett. **68**, 2512 (1992).
[37] J. Fernández-Rossier, Phys. Rev. Lett. **102**, 256802 (2009).
[38] F. Delgado and J. Fernández-Rossier, Phys. Rev. B **82**, 134414 (2010).
[39] Y. Fang, S. Chesi, and M.-S. Choi, Phys. Rev. B **104**, 195122 (2021).
[40] R. Korytár and N. Lorente, J. Phys.: Condens. Matter **23**, 355009 (2011).
[41] D.-J. Choi, P. Abufager, L. Limot, and N. Lorente, J. Chem. Phys. **146**, 092309 (2017).
[42] X. W. Tu, G. R. Mikaelian, and W. Ho, Phys. Rev. Lett. **100**, 126807 (2008).
[43] J. Kim, K. Noh, Y. Chen, F. Donati, A. J. Heinrich, C. Wolf, and Y. Bae, Nano Lett. **22**, 9766 (2022).
[44] X. Zhang, C. Wolf, Y. Wang, H. Aubin, T. Bilgeri, P. Willke, A. J. Heinrich, and T. Choi, Nat. Chem. **14**, 59 (2022).
[45] S. Kovarik, R. Robles, R. Schlitz, T. S. Seifert, N. Lorente, P. Gambardella, and S. Stepanow, Nano Lett. **22**, 4176 (2022).
[46] R. Kawaguchi, K. Hashimoto, T. Kakudate, K. Katoh, M. Yamashita, and T. Komeda, Nano Lett. **23**, 213 (2023).